Int J Earth Sci (Geol Rundsch) (2005) 94: 130–146
DOI 10.1007/s00531-004-0442-3

ORIGINAL PAPER

Fritz Neuweiler · Daniel Bernoulli

Mesozoic (Lower Jurassic) red stromatactis limestones from the Southern Alps (Arzo, Switzerland): calcite mineral authigenesis and syneresis-type deformation

Received: 24 November 2003 / Accepted: 27 August 2004 / Published online: 28 October 2004

Abstract The Broccatello lithological unit (Lower Jurassic, Hettangian to lower parts of Upper Sinemurian) near the village of Arzo (southern Alps, southern Switzerland) is a mound-shaped carbonate deposit that contains patches of red stromatactis limestone. Within the largely bioclastic Broccatello unit, the stromatactis limestone is distinguished by its early-diagenetic cavity system, a relatively fine-grained texture, and an in-situ assemblage of calcified siliceous sponges (various demosponges and hexactinellids). A complex shallow subsurface diagenetic pathway can be reconstructed from sediment petrography in combination with comparative geochemical analysis (carbon and oxygen isotopes; trace and rare earth elements, REE + Y). This pathway includes organic matter transformation, aragonite and skeletal opal dissolution, patchy calcification and lithification, sediment shrinkage, sagging and collapse, partial REE remobilization, and multiple sediment infiltration. These processes occurred under normal-marine, essentially oxic conditions and were independent from local, recurring syn-sedimentary faulting. It is concluded that the stromatactis results from a combination of calcite mineral authigenesis and syneresis-type deformation. The natural stromatactis phenomenon may thus be best explained by maturation processes of particulate polymer gels expected to form in fine-grained carbonate sediments in the shallow subsurface. Conditions favorable for the evolution of stromatactis appear to be particularly frequent during drowning of tropical or subtropical carbonate platforms.

Keywords Stromatactis · Carbonate mound · Mesozoic · Jurassic · Switzerland

F. Neuweiler (✉)
Department of Geochemistry, Geoscience Center,
University Göttingen, Goldschmidtstrasse 1,
Göttingen, 37077, Germany
E-mail: fneuwei@gwdg.de or fritz.neuweiler@ggl.ulaval.ca

D. Bernoulli
Department of Earth Sciences, University of Basel,
Bernoullistrasse 32, Basel, 4056, Switzerland
E-mail: daniel.bernoulli@unibas.ch

Present address: F. Neuweiler
Institute for Paleontology, University Erlangen,
Loewenichstrasse 28, Erlangen, 91054, Germany

F. Neuweiler
Département de géologie et génie géologique,
Pavillon Pouliot, Université Laval,
Québec, G1K 7P4, Canada

Introduction

The red stromatactis limestones that form deep-water, fine-grained carbonate mounds are generally considered typical of the Palaeozoic because they were first recognized in Palaeozoic limestones and because of their most obvious and spectacular occurrences in these rocks (Bathurst 1982; James and Bourque 1992). The term "stromatactis" was originally coined by Dupont (1881) for occurrences in the Upper Devonian red limestones of the Belgian Ardennes (Fig. 1a), and was later redefined by Lecompte (1937, 1954). Revisiting Dupont's classical localities, Bourque and Boulvain (1993) presented an emended definition for stromatactis as a "spar network, whose elements have flat to undulose smooth lower surfaces and digitate upper surfaces, made up principally of isopachous crusts of centripetal cement and embedded in finely crystalline limestone". Stromatactis is thus defined by its shape, three-dimensional network, host sediment, and centripetal (or drusy) cement fabric (Fig. 1a). Stromatactis occurs frequently but not exclusively within a host of red limestone, and is common in large mound structures from Cambrian to Carboniferous outer carbonate ramp environments (e.g., Ross et al. 1975; Bourque and Gignac 1983; James and Gravestock 1990; Bourque and Boulvain 1993; Lees and Miller 1995; Boulvain 2001).

The apparent limitation of stromatactis to the Palaeozoic suggested a biological origin reflecting evolution/innovation, geographical spread, and subsequent

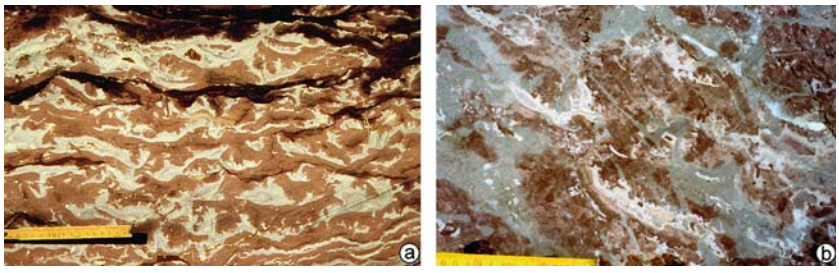

Fig. 1 Devonian and Jurassic red stromatactis limestones compared. **a** Upper Devonian (Frasnian) red stromatactis limestones from the Belgian Ardennes. This example substitutes, in a stratigraphic and structural sense, Dupont's original material (Boulvain, personal communication). **b** Lower Jurassic (Sinemurian) red stromatactis limestone from Arzo quarry (southern Alps, Switzerland). Compared to their Palaeozoic counterpart, the Jurassic stromatactis are generally smaller in size and of lesser lateral extent. Note the varying degrees of internal sediment fill versus cement precipitation. Field photographs, scale in centimeters

decline and extinction of an organism or a group of closely related forms (e.g. Dupont 1881; Lecompte 1937; Tsien 1985; Flajs and Hüssner 1993; Wendt et al. 2001). In contrast, Lees (1964, p. 518ff), Bourque and Gignac (1983), Bourque and Boulvain (1993), and Neuweiler et al. (2001a) favored a nonreplacive, early diagenetic opening of a cavity system that is in agreement with siliceous sponge taphonomy and organic matter diagenesis. Other authors argued for a mechanical origin of stromatactis considering it as a sedimentary structure either due to burrowing (Shinn 1968) or to internal reworking and erosion (Heckel 1972; Bathurst 1982 pro parte; Wallace 1987). Stromatactis, stromatactoid or stromatactis-like structures were also discussed in a scenario of seepage of light hydrocarbons (e.g., methane fluids, Hovland et al. 1987; Peckmann et al. 2002) or even gas clathrate hydrate formation and dissociation (CO_2-gas hydrate, Krause 2001). These views are so radically different that one could get the impression that either the scientific community uses the term stromatactis inconsistently, or indeed, stromatactis is not a specific geological phenomenon and, in contrast to the actually convincing arguments of Bathurst (1982), the different occurrences do not share a common origin.

In this paper, we present the case of a Mesozoic (Lower Jurassic) red stromatactis limestone (Fig. 1b), which occurs in an environment of recurring syn-sedimentary tectonic events, including extensional faulting, fracturing, and neptunian dyke formation typical of an active rift setting. Although the mounds and the stromatactis cross-sections are much smaller in size compared to their Palaeozoic counterparts (Fig. 1), we show that: (a) petrographically, these occurrences match the original and emended definition of stromatactis, (b) geochemically, the host limestone and the stromatactis calcite spar exclusively record normal-marine conditions, (c) by its fabric complexity, geochemistry, and occurrence, stromatactis represents a specific natural phenomenon, and that (d) stromatactis mirrors a complex pathway of organically thriven, chemical and physical diagenesis, including the decay of organic tissues, shrinkage, calcification, and collapse of sediment, rather than a simple biological, mechanical, seepage- or gas clathrate-related origin.

Location, previous work, and geological setting

Field work was performed in quarries NE of Arzo, southern Alps, southern Switzerland (Fig. 2). Here, the Triassic (Norian Hauptdolomit) to mid-Liassic (pelagic limestones) rock sequence represents a tectono-sedimentary history of tropical carbonate platform deposition, followed by subaerial exposure, erosion, platform drowning, and neptunian dyke and breccia formation (Wiedenmayer 1963). The Arzo locality represents one of several spectacular examples of Jurassic extensional syn-sedimentary tectonics (Bernoulli et al. 1990; Winterer et al. 1991), but none of them yielded evidence for an episode of hydrothermal circulation as proposed, e.g., by Hsü (1983).

Stromatactis limestones occur within the Broccatello unit (Liassic, essentially Lower Sinemurian), a fossiliferous, varicolored (''brocade'') to reddish limestone formation mapped in detail by Wiedenmayer (1963), and commonly compared to the Hierlatz facies of the Northern Calcareous Alps (e.g., Frauenfelder 1916). The Broccatello has been inferred to have a ''biohermal'', ''lithohermal'' or mound-shaped geometry (Wiedenmayer 1963, 1980; Bernoulli 1964; Bernoulli in Baumgartner et al. 2001). Although detailed sedimentological work was done in the Arzo quarries (Wiedenmayer 1963; Winterer et al. 1991), it was not before Bernoulli (in Baumgartner et al. 2001) that ''stromatactis-type'' cavities within the Broccatello limestone were mentioned. The Broccatello limestones that contain stromatactis are best exposed at present in the small, active quarry immediately east of locations 6 and 7 of Baumgartner et al. (2001, their Fig. 13).

The regional palaeogeographic setting of the Arzo locality (Figs. 2, 3) relates to the marginal area of a Jurassic submarine high (Lugano or Arbostora High), close to the fault scarp separating a higher footwall-block from the hanging-wall block of the strongly subsiding Monte Generoso Basin (Bernoulli 1964; Bernoulli et al. 1990; Bertotti et al. 1993). On a larger scale (Fig. 3), the Arzo locality was situated within a large rift basin, the Lombardian Basin, evolving during early rifting along the proximal margin of the Adriatic micro-

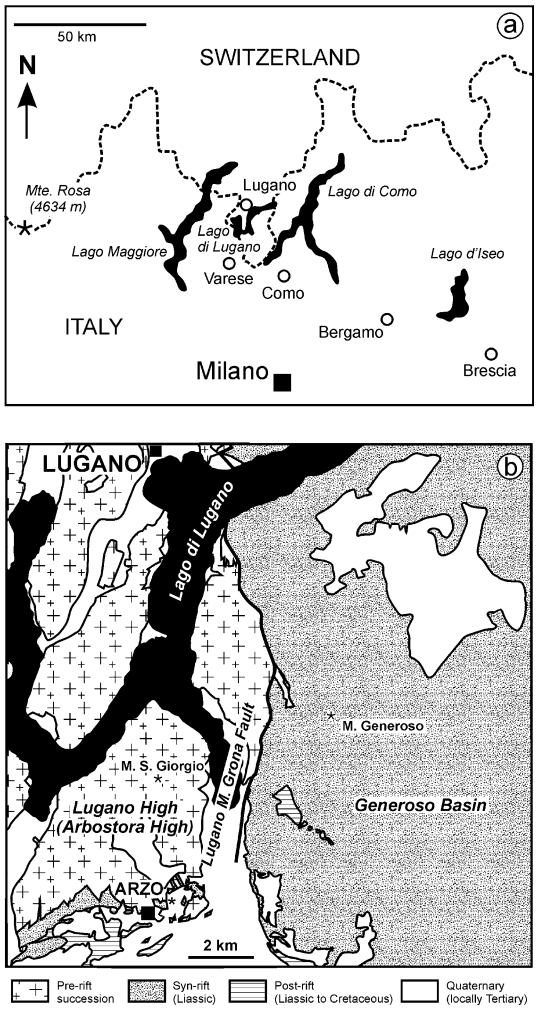

Fig. 2 Location and structural setting of the Arzo area, south of Lugano, Switzerland. The Arzo area is marked by syn-sedimentary tectonic fragmentation along the eastern margin of the Lugano High. The Lugano-Monte Grona fault represents the main zone of syn-sedimentary faulting separating the Lugano High from the Generoso basinal trough. Geological map simplified from Bernoulli (1964); lakes shown in *black*

plate. The rapidly subsiding rift basins contain an enormous amount of biosiliceous hemipelagites (Moltrasio Formation or Lombardischer Kieselkalk, up to 3.5 km thick), whereas on the adjacent submarine highs a relatively thin, partially condensed, deepening-upward succession was laid down. On the Lugano High, platform drowning occurred during the Triassic-Jurassic boundary interval, leading to the formation of an intrabasinal high on which, from the middle Liassic onwards, pelagic conditions prevailed culminating during the middle to late Jurassic with the deposition of carbonate-free radiolarites. During the Liassic interval, the inferred palaeolatitude was around 30°N (based on Golonka 2000).

This paper deals with the intermediate facies of the Broccatello unit, intercalated between Rhaetian carbonate platform and middle Liassic pelagic deposits (Rosso Ammonitico facies s.l.), containing both biocarbonate (brachiopod) and biosiliceous (sponge) epibenthos. Such transitional facies are rarely exposed; possible analogues are the siliceous sponge-rich Misone Limestone from the western margin of the Trento platform (Castellarin 1972; Krautter 1996) and the Lower Liassic limestones of the Gozzano High resembling the Broccatello (Montanari 1969).

Materials and methods

Rock samples were collected for both petrographic analysis and geochemical sampling from slabs. These samples for geochemistry include (Table 1) in-situ precipitated microcrystalline calcite (automicrite) from calcified sponges, geopetal micrite (allomicrite), and early cement and late blocky spar cement taken from stromatactis and a brachiopod filling, respectively. Further samples comprise bulk crinoidal grainstone, bioclastic wackestone, a phosphorite, and a Domerian marly limestone. Carbon and oxygen stable isotopes were analyzed at the Laboratory of Stable Isotope Geochemistry at the Earth Science Department at ETH Zürich. Analyses were performed using an on-line common bath coupled to a VG PRISM mass spectrometer. The analytical precision of the mass spectrometer is ± 0.1 or better for $\delta^{13}C$, and ± 0.1 or better for $\delta^{18}O$. All the $\delta^{18}O$ values have been corrected for calcite phosphoric acid fractionation. The $\delta^{13}C$ and $\delta^{18}O$ values are given in the V-PDB notation. Trace elements with rare earth elements + yttrium (REE + Y) were determined on aliquots using a Fisons PQ 2 + ICPMS (inductively-coupled plasma mass spectrometry) of the Geochemistry Department at Göttingen University. Sample preparation was performed with HNO_3. Measurements of element concentrations have a

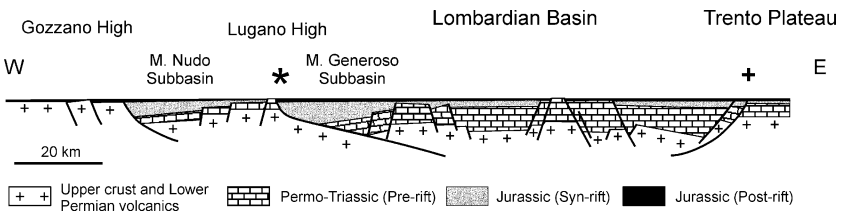

Fig. 3 Reconstructed geological cross-section of the Lombardian Basin for the Late Jurassic. The Arzo locality (asterisk) marks the boundary zone between the Monte Generoso Subbasin and the Lugano High (Lugano-Monte Grona fault). Siliceous sponge facies also occur at the eastern boundary (+) of the Lombardian Basin close to the Garda escarpment. Summarized after Bertotti et al. (1993) and Manatschal and Bernoulli (1999).

Table 1 REE, Y, Zr content (in ppm) and $\delta^{13}C$, $\delta^{18}O$ values (‰ versus Vienna-PDB) of Liassic stromatactis facies with its fabric elements (automicrite, allomicrite, marine cement, drusy calcite cement) and adjacent sedimentary facies (crinoidal grainstones, bioclastic wackestones, phosphorites, Domerian marly limestone)

	Broccatello biohermal				Broccatello crinoidal			U. Sinemurian in Broccatello	Domerian in Broccatello	Burial diagenesis
	Automicrite-1 (calcified sponge)[a]	Automicrite-2 (calcified sponge)[b]	Allomicrite-1 (brachiopod internal sed.)[c]	Allomicrite-2 (stromatactis internal sed.)[a]	Crinoidal grainst. (from dyke)	Marine cement (from stromatactis)[b]	Bioclastic wackestone	Phosphorite (from dyke)	Marly limestone (from dyke)[b]	Drusy calcite cement (from brachiopod)[c]
La	1.86	1.94	4.18	1.40	3.05	0.82	4.55	6.60	4.80	0.73
Ce	1.84	1.88	4.42	1.38	2.65	0.49	5.11	5.61	7.38	0.81
Pr	0.36	0.38	0.79	0.28	0.58	0.14	0.89	1.18	1.11	0.14
Nd	1.43	1.38	3.00	1.05	2.44	0.51	3.48	4.65	4.29	0.59
Sm	0.26	0.28	0.61	0.25	0.50	0.12	0.68	0.86	0.81	0.12
Eu	0.05	0.07	0.13	0.05	0.13	0.03	0.15	0.19	0.19	0.03
Gd	0.29	0.30	0.63	0.25	0.68	0.19	0.77	1.03	0.91	0.18
Tb	0.04	0.05	0.09	0.04	0.10	0.03	0.10	0.15	0.13	0.03
Dy	0.29	0.32	0.55	0.24	0.63	0.18	0.63	1.02	0.87	0.18
Y	2.69	2.33	5.38	1.96	6.35	2.74	5.70	12.07	6.03	2.08
Ho	0.06	0.07	0.13	0.05	0.15	0.05	0.15	0.24	0.17	0.05
Er	0.18	0.20	0.39	0.15	0.40	0.14	0.40	0.71	0.49	0.15
Tm	0.03	0.03	0.06	0.03	0.06	0.03	0.06	0.11	0.07	0.02
Yb	0.16	0.17	0.30	0.13	0.37	0.15	0.31	0.59	0.37	0.12
Lu	0.03	0.03	0.05	0.02	0.06	0.03	0.06	0.11	0.07	0.02
Zr	3.52	3.48	8.12	2.61	2.62	1.27	10.05	4.84	15.68	0.65
$(Ce/Ce^*)_{SN}$	0.52	0.50	0.56	0.51	0.46	0.33	0.59	0.46	0.74	0.59
Y/Ho	46.2	34.2	40.8	38.0	42.9	51.5	39.3	51.2	35.4	41.7
$(Nd/Yb)_{SN}$	0.74	0.70	0.82	0.69	0.55	0.28	0.93	0.65	0.95	0.40
$(Sm/Yb)_{SN}$	0.83	0.86	1.03	1.00	0.69	0.38	1.11	0.74	1.10	0.52
$(Dy/Pr)_{SN}$	1.53	1.59	1.31	1.66	2.05	2.36	1.33	1.63	1.48	2.43
$\delta^{13}C$	2.4	2.3	2.6	2.5	2.5	2.5	2.3	1.8	1.2	2.6
$\delta^{18}O$	−0.1	−0.3	−0.5	−0.3	−0.6	−0.8	−1.0	−1.3	−2.8	−4.5

Superscript letters refer to geochemical samples collected from the same hand specimen.
SN shale-normalized (PAAS)

maximum error of 10% compared to a known international standard (JA-2) and lab carbonate standard (KK). Quantification is based on a blank substracted five-point calibration-curve using internal standardization by elements such as Be, Ge, Rh, In, Re, and Bi. Values of REE + Y patterns were normalized (REE_n) to average post-Archean Australian shale (PAAS). Anomalies in REE_n patterns were quantified by the ratio of the observed abundance to an expected value (REE*) interpolated for a smooth pattern from neighboring REEs; e.g., the Ce anomaly is quantified as $(Ce/Ce^*)_n = Ce_n/(La_n \times Pr_n)^{0.5}$.

Data from both methods independently serve to discriminate between normal-marine conditions and conditions influenced by subsurface fluids. Isotopic composition potentially indicates sulphate reduction or methane oxidation via negative deviations of $\delta^{13}C_{carbonate}$ (Beauchamp and Savard 1992; Hendry 1993), and hydrothermal fluids via negative deviations of $\delta^{18}O$ (e.g. Nesbitt 1996). The REE + Y geochemistry provides a redox tracer via the type and degree of the cerium anomaly in combination with the general shape of the REE distribution pattern (e.g., De Baar et al. 1988; MacLeod and Irving 1996; Haley et al. 2004), and an independent indicator of hydrothermal fluid flow via the type and degree of the europium anomaly (McLennan 1989). Some trace elements (zirconium, hafnium) in combination with the yttrium/holmium ratio are used to assess terrestrial versus marine signatures (Bau 1996) and the degree of yttrium fractionation in the marine environment (Bau et al. 1996).

Results

Sequence of lithofacies

At Arzo, a combination of the following factors allow for reconstructing a synthetic stratigraphic section (Fig. 6): the vertical succession as observed in the outcrop (Fig. 4), data extracted from the geological maps of Wiedenmayer (1963), and the cross-cutting relationships of neptunian dykes and related sediment fills (Fig. 5). At least seven successive events of dyke formation can be distinguished, ranging from subhorizontal cracks to subvertical dykelets with injection features (Fig. 5). The dykes may penetrate several tens of meters into the Norian Dolomite Formation (Hauptdolomit) where they might produce multiple cemented tectono-sedimentary breccias (so-called Macchia Vecchia). For the purpose of this paper, the following units are considered (Fig. 6, from base to top):

a. The Rhaetian dolomitic limestones (Tremona series, Kälin and Trümpy 1977) represent a Late Triassic peri-tidal to lagoonal depositional environment. The contact with the Liassic Broccatello is an angular unconformity, which includes dolomitization, subaerial exposure, and erosion (Wiedenmayer 1963).
b. The "biohermal Broccatello" is a varicolored ("brocade"), reddish, massive limestone rich in brachiopods and calcareous sponges. Fragments of crinoids are ubiquitous, and some solitary corals occur. This unit contains patches of red stromatactis limestone.
c. The "crinoidal Broccatello" is essentially an encrinite with wackestone to grainstone texture. The coloration varies from reddish, pink, violet, and beige. In the lower, micritic-pelletoidal part of the unit, calcareous sponges are present. The middle part is a marine-cemented grainstone interval, and the upper part is a wackestone with fragments of crinoids and some calcareous sponges. In the Arzo quarries, the Broccatello is essentially dated as Sinemurian up to the *Asteroceras obtusum* zone. However, similar facies of the Hettangian age are reported to occur as blocks in the Domerian marly limestones near the village of Arzo (Wiedenmayer 1963, p. 508).
d. The phosphorites occur only within the dyke system exposed at the floor of one of the quarries (small, active quarry east of 6 and 7, Fig. 13 in Baumgartner et al. 2001). They form subangular to rounded components enclosed within a matrix of reddish crinoidal wackestone and/or grainstone ("Crinoidal Broccatello"). Small clasts of phosphorite nodules, in association with glauconite, were described from condensed Upper Sinemurian encrinites overlying the Norian Hauptdolomit west of Arzo (locality Burgioli, Wiedenmayer 1963). In the Arzo quarries, the condensed section presumably grades into a hiatus, as deduced from the regional lack of corresponding ammonites, which would represent the youngest parts of the Sinemurian (zones of *Oxynoticeras oxynotum* and *Echioceras raricostatum*, Wiedenmayer 1963).
e. The Besazio Limestone (Carixian to lower Domerian) is a fairly homogeneous, micritic limestone with cephalopods, crinoids, and brachiopods. It typically contains shelly fragments surrounded by crusts of Fe- and Mn-oxihydroxides. Locally, bundles of *Apiocrinus* holdfasts occur (Wiedenmayer 1963, 1977).
f. The marly limestones of late Pliensbachian (Domerian, Morbio Formation) age are brick-red to deep-red, locally rich in crinoids, and sporadically including faint carbonate nodules, and thus are transitional to the Rosso Ammonitico lithology.

Red stromatactis facies within the Broccatello

Lithology and geometry

The original thickness and depositional geometry of the Broccatello unit are difficult to establish because both attributes have been influenced to a large extent by the syn-sedimentary extensional tectonics (Fig. 7). The maps and cross-sections of Wiedenmayer (1963) suggest that the maximum thickness is reached in the area of the Arzo quarries, east of a high with reduced and con-

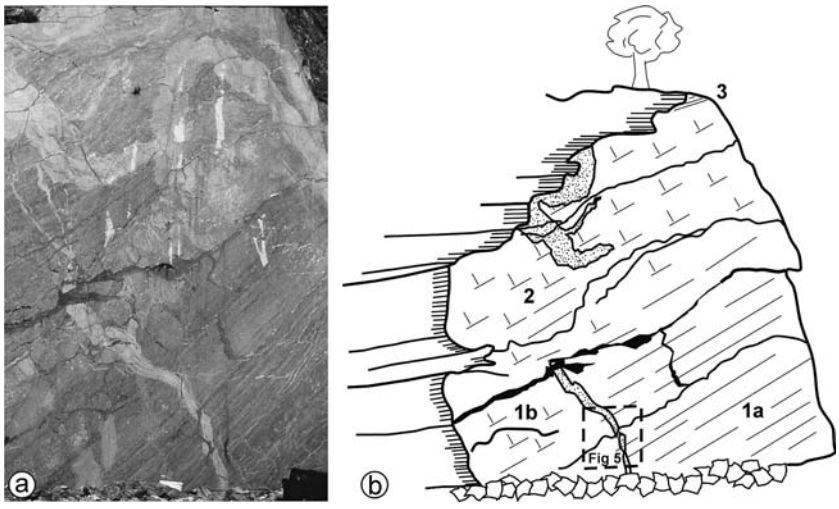

Fig. 4 Main outcrop of the Lower Jurassic Broccatello unit exposed in the active quarry NE of Arzo. **a** Outcrop photograph exposing vertical facies succession and composite sets of neptunian dykes. **b** Schematic drawing (highly simplified, lower dyke of crinoidal grainstone for orientation).The main lithofacies encompass a red bioclastic limestone rich in brachiopods and calcareous sponges (1a), patches of red stromatactis limestones (1b), varicolored crinoidal limestones, mainly grainstones (2), and grey bioclastic wackestones (3)

densed sedimentation. To the east, i.e., towards the Generoso Basin, the Broccatello unit pinches out over a distance of about 1 km and is overlain with an onlap of the basinal Moltrasio Formation. East of the Lugano-Monte Grona fault, the Broccatello unit is present as olistoliths in the Moltrasio Formation (Bernoulli 1964). Based on the present-day distribution of its occurrences in the different faulted blocks, it appears that it had a relatively flat mound-shaped geometry with a maximum thickness in the 50 m range.

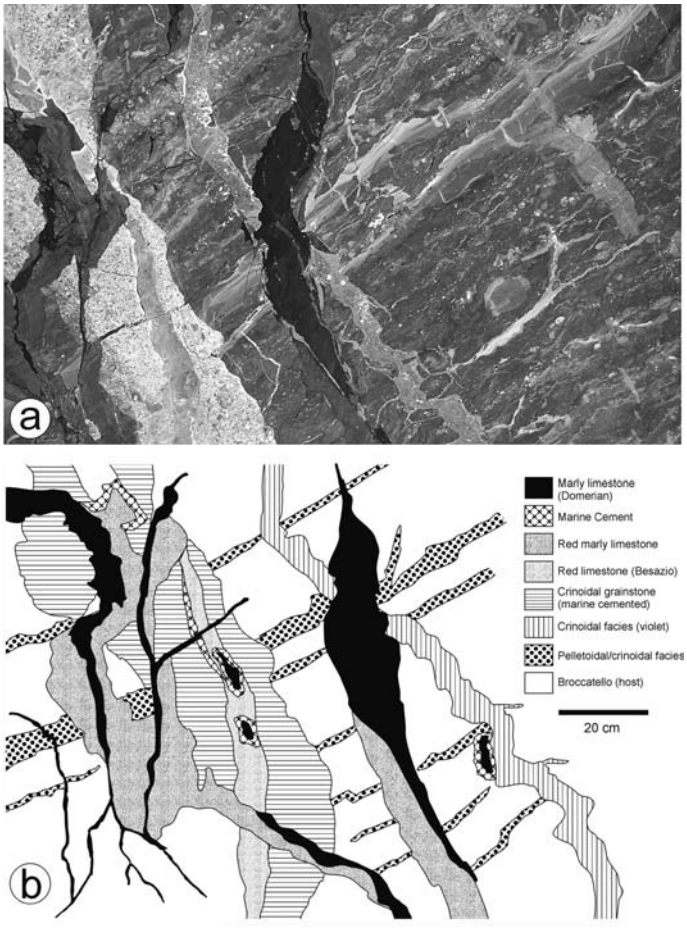

Fig. 5 Cross-cutting relationships within the system of sheet cracks and neptunian dykes, Arzo quarry, Broccatello (Lower Sinemurian) to Pliensbachian (Domerian) marly limestones. The first generation corresponds to en-echelon fractures subparallel to bedding similar to simple-shear Riedel-shear planes. Subsequent generations tend to be subvertically curved (crinodial facies) or subvertical dilational cracks. Domerian marly limestones are found in millimeter-thin, multiple branching dykelets suggesting injection rather than infiltration of sediment material. See Wiedenmayer (1963) and Winterer et al. (1991) for further examples

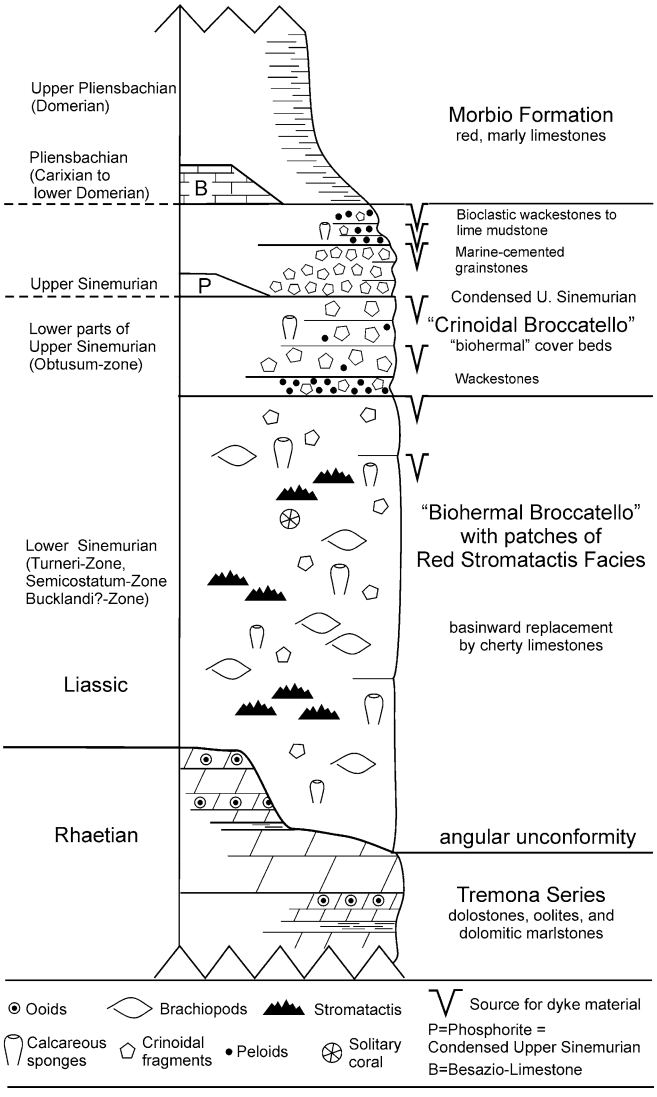

Fig. 6 Synthetic stratigraphic section of the Liassic succession at Arzo. Stromatactis facies occur within the lower part of the Broccatello unit, which is covered by crinoidal sands. The upper part of the succession is reconstructed from the facies sequence in the sedimentary dykes as defined by their cross-cutting relationships (compare Fig. 5). Semiquantitative illustration of succession of facies, not to scale

The Broccatello contains abundant and diverse terebratulid and rhynchonellid brachiopods (Fig. 8; at least seven brachiopod genera were reported by Wiedenmayer 1963, including *Zeilleria* and *Spiriferina*), crinoidal debris, pharetronid sponges (*Stellispongia*, *Corynella*, see Wiedenmayer 1963), shells of pectinid and ostreid bivalves, and some solitary corals and bryozoan fragments.

The red stromatactis limestone forms a massive sublithofacies within the Broccatello (Fig. 9), being enclosed within a mound-shaped, brachiopod-rich bioclastic limestone. The thickness of this sublithofacies ranges from several tens of centimeters to several meters with an overall patchy distribution and lacking any significant syndepositional relief. Individual patches (Fig. 9a) are lense- to mound-shaped, and have gradational contacts to the surrounding Broccatello. Occurrences of stromatactis within a relatively fine-grained host rock, and of mesoscopic (hand-lens) sponge spicule networks are the only distinguishing characters with respect to the surrounding facies.

The size of stromatactis cross-sections is in the centimeter range with maxima at around 10 cm in width and 2 cm in height. The occlusion of the primary stromatactid cavity network has been achieved by a spectrum of fillings ranging from cement only (stromatactis), to incipient marine cementation followed by internal sediment (inhibited stromatactis), and to internal sediment only (aborted stromatactis) as described in Neuweiler et al. (2001a). Proportionally, stromatactis is as abundant as inhibited and aborted stromatactis taken together (Fig. 1b, 9). Abortion of stromatactis occurs due to early plugging of the cavity system prior to marine cement precipitation by Sinemurian internal sediment, whereas inhibition occurs via the infiltration of Domerian marly material subsequent to the development of only minor crusts of marine cement.

Microfabric

The red stromatactis limestone is essentially a bioclastic wackestone with an in-situ assemblage of calcified siliceous sponges (Fig. 10). The siliceous sponges comprise lithistid and non-lithistid demosponges as well as hexactinellid sponges represented by Lyssacinosa and Hexactinosa (Fig. 11). The sponges were only partially calcified, became fragmented to a variable degree and/or were subject to bioerosion or excavation during their calcified stage (Fig. 11d). The bioclastic sediment consists of crinoidal debris, gastropods (including archaegastropods of the type *Discohelix* and *Pleurotomaria*), terebratulid and rhynchonellid brachiopods, bivalve shells, and some calcareous sponges, fragments of dendroid bryozoans, polychaete tubes (*Terebella*), and benthic foraminifera (*Involutina liassica*). The micritic matrix is fairly homogenous hosting microbioclasts, small intraclasts, and the ubiquitous ostracods. Some of the skeletal (mainly molluscan) debris was affected by microborings and impregnation of Fe-oxide coatings.

The internal geopetal sediment of the stromatactid cavity system is a fine-grained lime mudstone to grainstone with microbioclasts and pellets or small intraclasts. Current-induced sediment deposition is evident from inverse grading, abrasion of small intraclasts, and locally low-angle cross-lamination (Fig. 12b).

Early diagenesis

Early lithification of the Broccatello limestone is documented by the brittle behavior of the limestones during penecontemporaneous tectonic fracturing and neptunian dyke formation. The main aspects of the early diagenesis of Liassic stromatactis facies include (in chronological order):

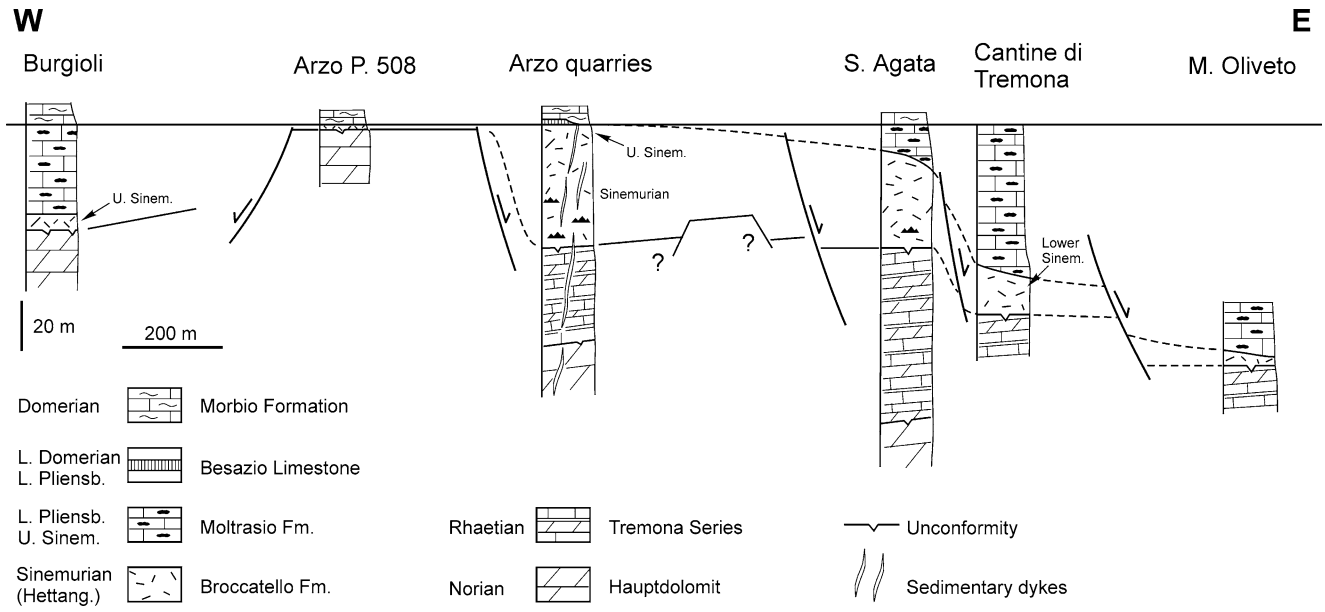

Fig. 7 Depositional geometry of the Sinemurian Broccatello unit. Our reconstruction is based on the map and the sections of Wiedenmayer (1963). The depositional geometry is largely defined by syn-sedimentary faulting. West of the quarries of Arzo (P. 508), the Broccatello is preserved as very small relics and as blocks in the Morbio Formation and rests directly on Hauptdolomit. East of the quarries, the formation appears to pinch out towards the Generoso basin. Its top, Upper Sinemurian at Arzo, becomes older towards the east and at Cantine di Tremona is in the Lower Sinemurian (Wiedenmayer 1963). Near M. Oliveto, the Broccatello is reduced to a few meters only. West of the village of Arzo, current-bedded crinoidal limestones (Saltrio Beds) with a condensed, late Sinemurian ammonite fauna (Wiedenmayer 1963) at their base, overlie the Hauptdolomite with a phosphate-rich hardground

a. Siliceous sponge calcification
b. Skeletal opal dissolution in association with sponge fragmentation and collapse
c. Opening of the stromatactid cavity system
d. Aragonite dissolution
e. Obturation of the cavity system, by internal sediments and/or single or multiple crusts of marine cement

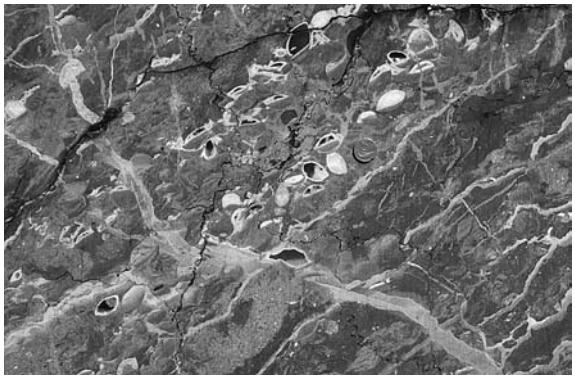

Fig. 8 Stratiform accumulations of brachiopods, some of which display tilted geopetal fabrics. Note details of the multiphase dykelet system, Broccatello unit, field photograph, diameter of coin 2.0 cm

Late diagenetic features comprise blocky calcite cement, subvertical and bedding-parallel stylolites, and subvertical fissures cemented by a second generation of blocky calcite (alpine veins).

Ad (a) Siliceous sponge calcification (Fig. 11) is a syn-vivo to early postmortem phenomenon affecting hexactinellids and demosponges (“Verwesungsfällungskalk” of Fritz 1958). It is only sporadically observed in Quaternary deposits (Froget 1976; Reitner et al. 1995), but is a common feature of Phanerozoic, deep-water siliceous sponge facies (e.g., Brunton and Dixon 1994). Petrographically, siliceous sponge calcification fabric displays a correlation between the early stages of soft tissue degradation and shrinkage patterns. The detailed mechanism of siliceous sponge calcification is still not clear: the role of ammonification was stressed by Fritz (1958), a matrix-mediated mineralisation process was proposed by Reitner et al. (1995), and humification was favored by Neuweiler et al. (2000, 2003). Sponge-specific microbial metabolism during decay was discussed by Reitner and Schumann-Kindel (1997) and Schumann-Kindel et al. (1997). Although hexactinellid soft tissue is largely devoid of a significant symbiotic bacterial biomass (Leys 1999), some associated eubacteria and Archaea could be present (Thiel et al. 2002).

Ad (b) Dissolution of the opaline spicular skeleton of siliceous sponges occurs pervasively, i.e., within and outside the calcified portions of the sponge (cf. Froget 1976). As tissue shrinkage resulted in only a patchy calcification, SiO_2-dissolution induces an entire set of early diagenetic features, namely skeletal dissolution, in-situ collapse, and fragmentation (Figs. 10, 11). Such fragmentation into calcified parts of siliceous sponges is well known, e.g., from Upper Jurassic spongiolithic limestones that may display sponge fragments (or tuberoids, sensu Fritz 1958) in rock-forming abundances (Flügel and Steiger 1981).

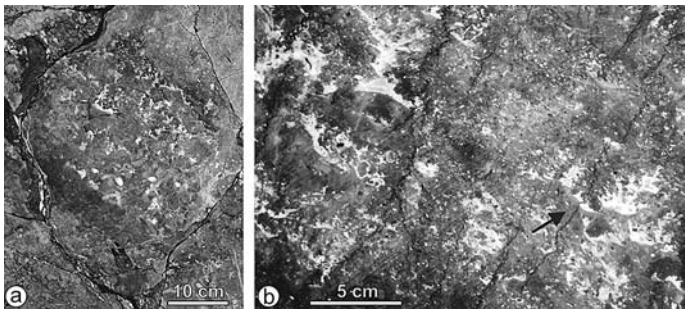

Fig. 9 Lower Jurassic stromatactis limestones of Arzo. **a** Patch of stromatactis limestone embedded within the Broccatello unit. The patch is approximately 70 cm in diameter, rich in brachiopods in its lower parts, and rich in stromatactis in its upper part. **b** Stromatactis within bioclastic wackestone. Tracing the relatively fine-grained internal sediment (*arrow*) provides an estimate of the original extent of the stromatactid cavity system

Ad (c) The opening of the stromatactid cavity system must be contemporaneous with the degradation and calcification processes described above, simply because fragments resulting from SiO_2 dissolution accumulated gravitationally within the stromatactid cavity system (Fig. 10). In fact, at the roof where the original cavity wall is not covered by internal sediment, shrinkage cracks are developed that pinch out from the stromatactid cavity into the cavity-supporting host (Fig. 10). Thus, the opening of the stromatactid cavity system mirrors siliceous sponge diagenesis in terms of decay of organic tissue, shrinkage, and calcification, the latter inducing induration of the host.

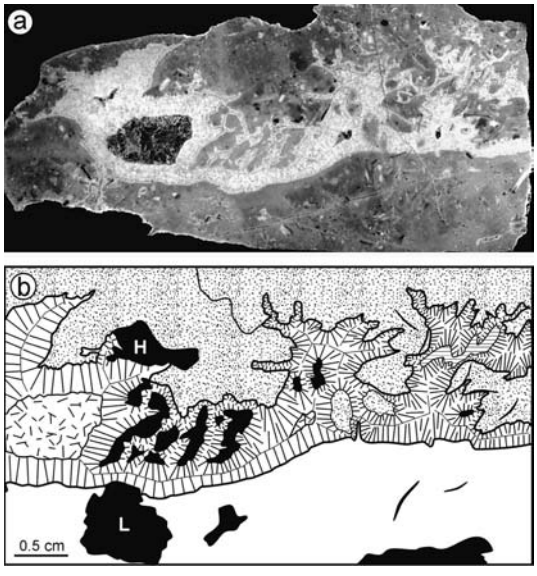

Fig. 10 Microfabric of Lower Jurassic stromatactis limestone. **a** View of polished slab, **b** schematic drawing from thin section made from same sample. Stromatactis is essentially a collapse feature (contraction) correlating with siliceous sponge diagenesis (calcified portion of siliceous sponges in black, *H* hexactinellids, *L* lithistid demosponges). Contractive cavity opening is associated with shrinkage cracks pinching out from the cavity towards the cavity supporting host. Subsequent sediment infiltration produced a polymud fabric (cf. Lees and Miller 1995)

Ad (d) Shallow subsurface dissolution of aragonite is evident from molluscan molds filled by geopetal microcrystalline carbonate sediment that also contributes to the early filling stages of the stromatactid cavities (Fig. 12a). Calcium carbonate dissolution must have been highly selective for aragonite because microborings remained stable as did precursor and subsequent internal sediments (Fig. 12a). Thus, in the shallow subsurface, aragonite molds were partially connected to the stromatactid cavity system within an indurated host of essentially fine-grained calcite mineralogy.

Ad (e) The various modes of obturation of the combined aragonite mold/stromatactid cavity system includes: (1) an always present internal sediment of micrite or microspar that may grade into fine-grained pelsparite with small intraclasts (Fig. 12). Common elements are bioclasts (crinoids, sponge spicules, molluscan, and brachiopod shell fragments, foraminifera (*Involutina*), and disarticulated valves of thin-shelled ostracods, (2) a cross-bedded pellet grainstone that is contemporaneous with the early stages of marine cement precipitation. Locally, the grainstone infiltration plugged the cavity network to produce inhibited stromatactis, and (3) Domerian marly limestone subsequent to multigeneration early cement precipitation, thus locally preceding and/or substituting for late blocky calcite cement.

The first cement generation is multigenerated and internally zoned (Fig. 11b). The first rim is about 200 μm thin and consists of an alternation of limpid and inclusion-rich layers that combine to form an isopachous crust of bladed calcite cement. The second rim is a multigeneration radiaxial fibrous cement up to 3 mm thick. It consists of a brownish inner zone and a grey inclusion-rich outer zone. The early rim cement is strongly fluorescent indicating entrapment of organic matter either as primary inclusions or during a later episode of hydrocarbon migration.

Geochemical patterns

Geochemical information (stable isotopes, REE + Y patterns) refers to ten samples (Table 1), taken from two hand specimens. Automicrite refers to in-situ calcified sponges, allomicrite to geopetal, internal sediment. The other samples represent: marine-cemented crinoidal grainstones, crinoidal wackestones, phosphorite nod-

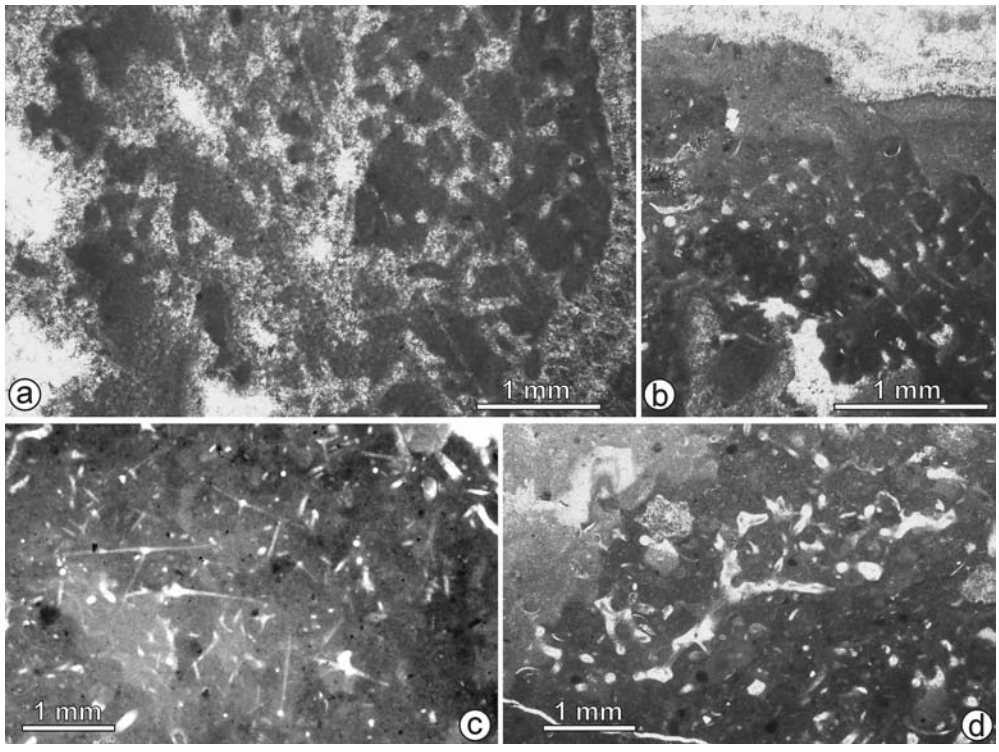

Fig. 11 Siliceous sponges from Lower Jurassic stromatactis limestones. **a** Calcified lithistid demosponge with subsequent marine cement on outer rims and within spicular molds, **b** Calcified hexactinellid sponge: Hexactinosa near the floor of stromatactid cavity sytem, **c** Calcified hexactinellid sponge: Lyssakinosa, **d** Calcified nonrigid demosponge with scalloped margins indicating bioerosion subsequent to calcification

ules, marine cement, Domerian marly limestone, and blocky calcite cement.

Stable isotopes

The $\delta^{13}C$–$\delta^{18}O$ scattergram of Fig. 13 integrates our own results (Table 1) and those of Winterer et al. (1991). The sediment (auto-allomicrite) and early rim cement values ($\delta^{13}C$ = 1.2–2.6‰ and $\delta^{18}O$ = −0.1 to −2.8‰) form a field clearly distinct from the field formed by the later blocky cement values ($\delta^{13}C$ = 1.9–2.7‰ and $\delta^{18}O$ = −3.7 to −8.6‰). The sediment-rim cement field falls in the early Jurassic marine calcite field as proposed by Veizer et al. (1999). The trend from the sediment-rim cement field to the blocky cement field is obviously one of progressive burial.

Our data are consistent with those of Winterer et al. (1991) who have already documented normal marine conditions for all Jurassic early diagenetic phases, and a burial origin for the blocky calcite cement of the central parts of cavities and the alpine veins. Minimum $\delta^{18}O$ values of late diagenetic blocky spar translate into a calculated burial temperature (assuming SMOW $\delta^{18}O_{water}$ = 0; cf. Kim and O'Neil 1997) of around 60°C. This appears reasonable in the light of independent evidence. Indeed, the clay mineral assemblage of the underlying Rhaetian limestones and dolomites represents the original detrital assemblage (Dunoyer de Segonzac and Bernoulli 1976), and the organic matter in the underlying Middle Triassic succession is immature and was never buried to temperatures exceeding 70 or 80°C (Bernasconi and Riva 1993). The data set shows some indications for a temporal decrease of $\delta^{13}C$ values separating Sinemurian carbonates from phosphorites and hemipelagic Pliensbachian marly limestones.

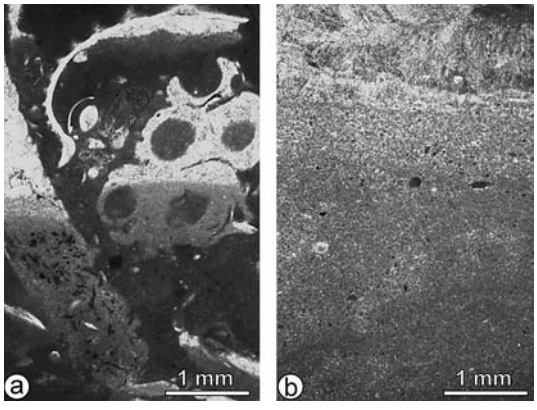

Fig. 12 Sediment infiltration and cement precipitation in Lower Jurassic stromatactis limestones. **a** Moldic porosity after former molluscan aragonite geopetally filled by infiltrated early diagenetic microcrystalline sediment. Note microendoliths not affected by the dissolution of the skeletal aragonite. **b** Inverse grading of geopetal internal sediment within stromatactid cavity system and exhibiting small intraclasts

Rare earth elements + yttrium

Although varying in absolute amounts, REE + Y patterns of the various facies and fabric elements (Fig. 14) are similar in general to each other in terms of: (a) distinctly negative Ce-anomalies, (b) superchondritic Y/Ho ratios (> 28) illustrated by the very distinct positive Y anomalies, and (c) relative enrichments in the heavy REE (Ho–Lu = HREE) with respect to the light

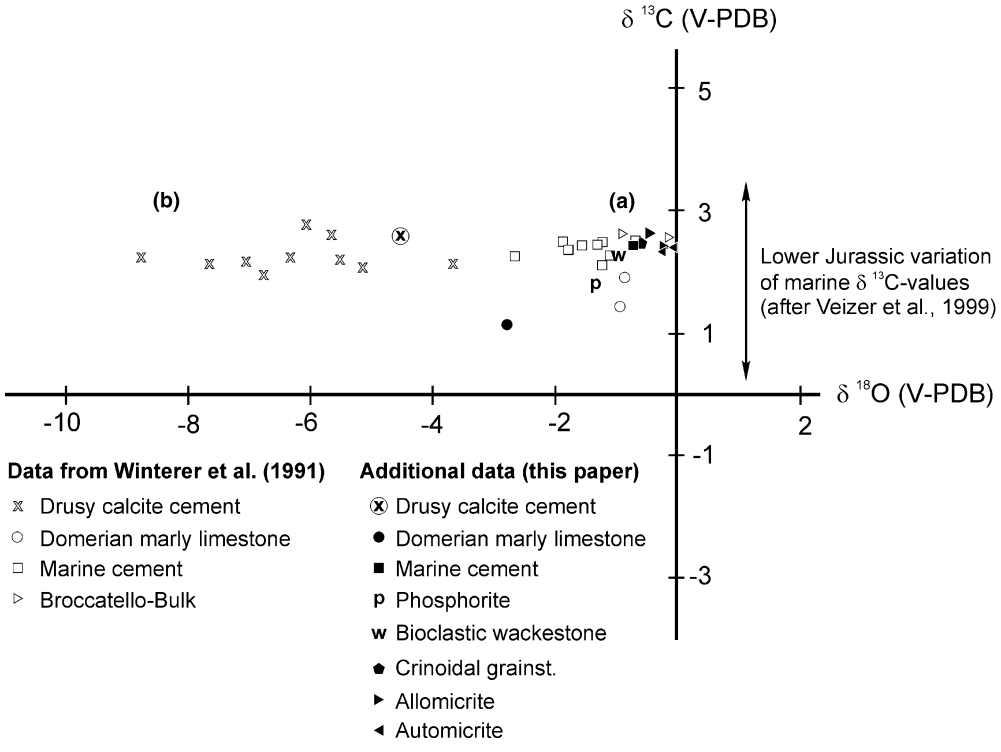

Fig. 13 Cross plot of $\delta^{13}C$ and $\delta^{18}O$ values (vs. Vienna-PDB in ‰) of the various sediments and cements of Liassic sediments at Arzo quarry. The pattern indicates a good quality of preservation separating well between two groups, **a** a scatter close to the expected marine values with minor temporal variation, and **b** a scatter mirroring elevated temperatures during burial diagenesis and the formation of alpine veins

REE (La–Nd = LREE). Within the gross range of middle REE (Pr–Dy = MREE), there is a well-developed range from relatively steep to relatively smooth patterns.

The values of the negative Ce-anomaly vary from a maximum of 0.32 for the marine cement to the least pronounced anomaly of 0.74 for the Domerian marly limestone. These values indicate, as it is commonly the case, marine-oxic conditions, as in its oxic state Ce^{4+} is usually adsorbed on Fe- and Mn-oxihydroxides, a marine sink for Ce which in turn results in a relative depletion (negative anomaly) of normal-marine waters (McLennan 1989).[1]

There is no significant Eu-anomaly for any of the measured samples. Values are around unity with minimum and maximum values for the two samples of automicrite (0.92–1.14). Although the detailed mechanisms for significant Eu anomalies is under debate, natural hydrothermal systems normally produce distinct positive Eu anomalies at low Y enrichments (Bau and Dulski 1999; Hongo and Nozaki 2001).

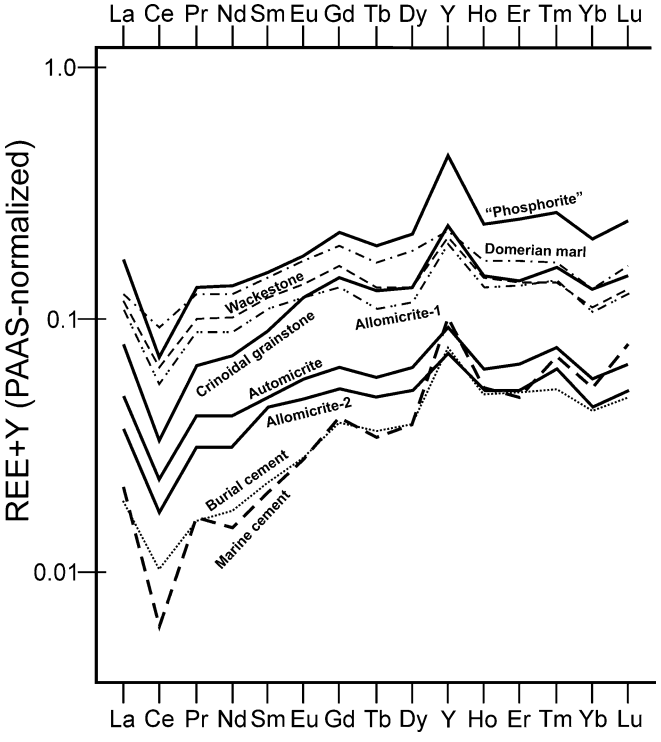

Fig. 14 PAAS-normalized REE + Y patterns of the various sediments and fabric elements of Liassic sediments at Arzo quarry. Although varying in absolute amounts, the patterns are similar to one another in terms of a negative Ce-anomaly, a superchondritic Y/Ho ratio, and relative enrichments of the heavy REE (Ho–Lu) over light REE (La–Nd). Note a rather continuous range of relative enrichment from Pr to Dy, i.e., from relatively steep (marine cement) to relatively smooth patterns (phosphorite, Domerian marl)

[1]The negative Ce-anomaly of automicrite (0.50 and 0.52) appears inconsistent with those values obtained from Cretaceous automicrites (positive anomaly and suboxic conditions, cf. Neuweiler et al. 2003 for details). It is beyond the scope of this paper to discuss the variation of REE patterns of fossil automicrites. It seems likely that for our case, sampling was not selective enough to obtain pure automicrites, but rather a mixture with marine cement (cf. Fig. 11a; see also Boulvain 2001). As an alternative, automicrite may also form under oxic conditions, but then appears to be much less pervasive compared to, e.g., massive sponge-automicrite mounds (Neuweiler et al. 2001b, 2003).

The Y/Ho ratio varies between a maximum value of 51 for the marine cement and the phosphorite down to a minimum value of 35 for the Domerian marly limestone. The Y/Ho ratio is a proxy to estimate the degree of terrigenous input into marine sediments, as in the marine environment Y is strongly fractionated from its geochemical twin Ho. Values >28 (value of PAAS) indicate that marine fractionation prevails over terrigenous input, whereas values >44 indicate rather pure marine conditions (Bau 1996). For all samples, Zr strictly covaries with Hf (97% Zr to 3% Hf, $R^2 = 0.98$), whereas only marly lithologies have absolute Zr contents >5 ppm (Fig. 15). Only for these samples Zr negatively correlates with Y/Ho-ratios indicating a terrestrial signature, whereas for ZrFig. 15). These rather pure sedimentary and diagenetic carbonates thus mirror fluctuating degrees of Y fractionation in the marine environment with maxima recorded for phosphorite and physico-chemically precipitated marine cement. Burial blocky spar shows a superchondritic Y/Ho ratio at minimum Zr contents indicating fluid flow mobilized from the adjacent marine limestones. Again, an unequivocal hydrothermal signature, e.g., relatively high Y contents at relatively low Y/Ho ratios (Bau 1996, his Fig. 6) is absent.

The relative enrichment of HREE over LREE can be quantified as the Nd(*n*)/Yb(*n*) ratio (*n* = shale-normalized). Enrichment is the strongest for the marine cement (0.28) and only minor (i.e., shale-like) for Domerian marls (0.95) with intermediate values, e.g., for the crinoidal grainstone (0.54), automicrite (0.71), and allomicrite (0.78). In addition, the range of relatively steep to relatively smooth middle REE patterns (quantified as Dy(*n*)/Pr(*n*)-ratio) is at its maximum values (>2) for burial and marine cement, and crinoidal grainstone, but relatively flat (<1.5) for both terrestrially influenced sediments and fully-marine, benthically produced materials (automicrite, phosphorite, allomicrite-2) (Fig. 16). According to the classical concept of the oceanic REE cycle (Elderfield and Greaves 1982), the relative enrichment of HREE occurs due to preferential scavenging of LREE in surface waters. Thus, sunken particles (inorganic and organic, enriched in LREE) are the only source to flatten the REE pattern via early diagenetic mobilization from the interstitial space of marine sediments (Elderfield and Greaves 1982; Cruse et al. 2000; Haley et al. 2004). Therefore, the Zr to Dy(*n*)/Pr(*n*) plot of Fig. 16 distinguishes well between "flat-terrigenous" or shale-like, "flat-marine" or benthic-diagenetic, and "steep-marine" or open-water REE patterns.

Discussion

Our data allow us to discuss: (1) to what degree the Lower Jurassic stromatactis limestones of Arzo match the Palaeozoic-type material, (2) how our case compares to other examples of Mesozoic stromatactis limestones, (3) how petrographic and geochemical constraints may lead to a deeper understanding of the origin of stromatactis, and (4) what significance stromatactis has for the interpretation of sedimentary to early diagenetic environments.

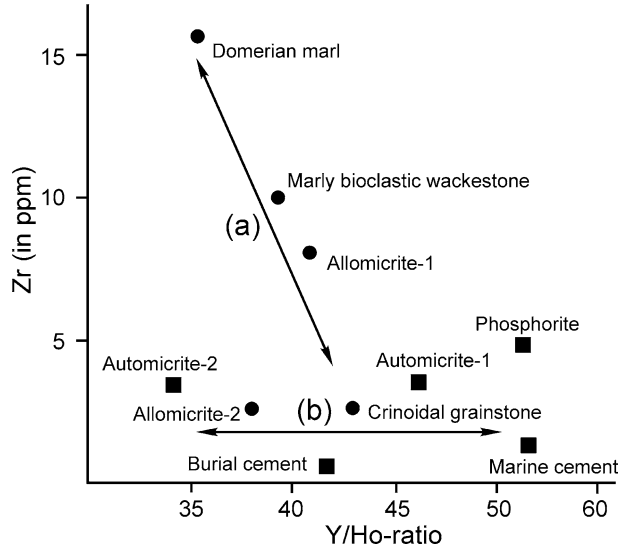

Fig. 15 Zr versus Y/Ho plot to discriminate between purely marine (e.g., marine cement) and terrigenously influenced endmembers (Domerian marl). The intersection of the regression line for terrigenously influenced sediments is near a Y/Ho ratio of 44 (indicated by *line a*), a gross value representing negligible contamination by, e.g., terrestrial detritus or volcanic ash that typically have chondritic Y/Ho values of around 28. Note highly variable degree of Y/Ho ratios under normal marine conditions (indicated by *line b*)

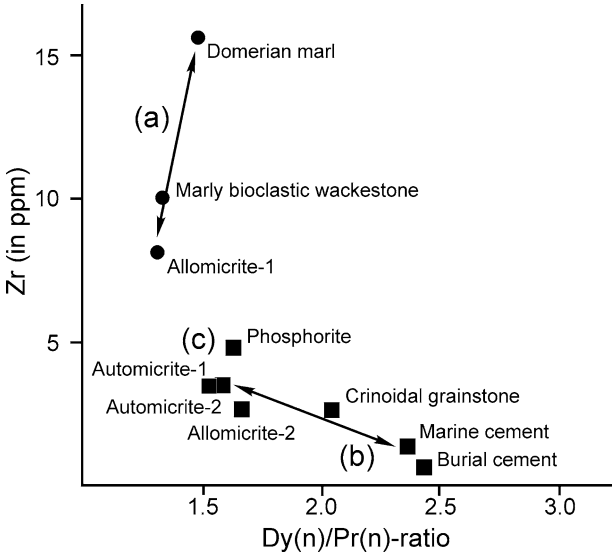

Fig. 16 Zr versus Dy/Pr plot to discriminate between relatively flat REE patterns (Dy/Pr around 1.5) either reflecting terrestrial input (**a**) or early diagenetic mobilization of relatively light REE within the interstitial under normal-marine conditions (**c**). Dy/Pr ratios >2.0 are in agreement with the more general heavy REE enrichment of marine, open waters (**b**)

Lower Jurassic and Upper Devonian stromatactis compared

As noted earlier, four diagnostic features are required for consistent use of the term "stromatactis", namely the network character, the shape, the presence of centripetal crusts of marine cement, and a fine-grained host.[2] The network character of Arzo stromatactis can be deduced from the uniform nature and distribution of the early internal sediment, some connective subvertical conduits, and successive plugging until the latest infiltrations by Domerian marl. As shown above, the stromatactid cavity system was connected locally to the system of moldic porosity as well as to the early subhorizontal fracture system. Thus, the cavity network evolved in the shallow subsurface prone to sediment infiltration and marine cement precipitation, and stayed connected to the surface (or locally became re-connected, e.g., by tectonic fracturing) down to several meters. The shape of Arzo stromatactis matches the flat to undulose smooth lower surfaces and digitate upper surfaces of the type material, and the same applies for the prescence of multiple crusts of marine cement. The only critical issue in terms of definition is the mean grain size of the host. Indeed, the Broccatello unit itself is a bioclastic wackestone (locally packstone) with some sand-sized allochems. Also, the microcrystalline matrix is not a homogeneous lime mud or pelletal mud, but includes bioclastic material at various amounts. However, well-defined patches of stromatactis limestones are essentially fine-grained and therefore fairly match the Palaeozoic type material.

Nonconstitutive characters of stromatactis (cf. Bathurst 1982), such as the size and lateral extent, clearly deviate from maximum values of Palaeozoic counterparts (Fig. 1 and Boulvain 1993). A relationship between neptunian dykes and stromatactis occurs only sporadically in Mesozoic (this paper) as well as in Palaeozoic stromatactis limestones (Bourrouilh et al. 1998). It does not establish a cause and effect but must be considered as an additional feature induced by loading or local extensional syn-sedimentary tectonics.

Interestingly, like in the Southern Alps, also along subsiding passive margins of the Palaeozoic stromatactis limestones are commonly intercalated between carbonate platform deposits below and a pelagic sequence above, deepening upward from stromatactis limestones to Rosso Ammonitico (Devonian Griotte) and radiolarites (Lower Carboniferous lydites), as, e.g., in the Montagne Noire (e.g. Bourrouilh et al. 1998 and references therein). Thus, and much like many siliceous sponge mounds in general, stromatactis limestones appear to represent an essential sedimentary-diagenetic option during the early stages of postdrowning intervals. Our current knowledge of mud-mound petrogenesis supports oceanographic rather than strictly bathymetric limiting parameters (e.g., Stanton et al. 2000; Boulvain 2001; Neuweiler et al. 2001b, 2003). However, taking the mixed layer as an upper limit (cf. review in Schlager 2003), tropical to subtropical settings provide a minimum depth in the (annual) mean range of 50 m (cf. Polovina et al. 1995; Bleck 2002 for theoretical considerations).

[2]Typical examples of Devonian stromatactis limestones can be leisurely studied in the men's room of the Geological Society, Burlington House, Piccadilly, London

Other examples of Mesozoic stromatactis limestones

Mathur (1975) has been the first to describe a Mesozoic red stromatactis limestone from the Jurassic of the Northern Calcareous Alps, and to suggest it is an analogue to the Palaeozoic "red stromatactis mud-mound". Unfortunately, the illustrations in Mathur (1975) do not allow a critical assessment, and the field evidence for stromatactis is rather poor (F. Neuweiler, personal observation). Better convincing Jurassic (Liassic) red stromatactis limestones from the Northern Calcareous Alps were later illustrated or mentioned by Mazullo et al. (1990); Böhm (1992) and Böhm et al. (1999: Langmoss Member of the Hettangian Schnöll-Formation). More recently, Neuweiler et al. (2001a) and Aubrecht et al. (2002) documented stromatactis limestones from the Cretaceous (Albian, Spain) and the mid-Jurassic (Bathonian to Callovian) of the Carpathian Pieniny klippen belt, Slovakia and Ukraine), respectively. Dromart et al. (1998) mentioned a low relief stromatactis mud-mound of Bathonian and Aalenian age from the Subalpine Basin of southeastern France.

Most of the above examples demonstrate a correlation between a siliceous sponge community or a spicule-bearing host and stromatactis fabrics. Nonetheless, and as it is the case for the Palaeozoic, a strict correlation does not exist (Boulvain 1993; Aubrecht et al. 2002). For example, Aubrecht et al. (2002) thought to have found stromatactis-type cavities within a host of a crinoidal packstone. Indeed, except for the fine-grained host, these examples match all the other constitutive elements of stromatactis, and they display vertical interfingering with fine-grained stromatactis limestones. Another important aspect stems from the Mid-Jurassic of the Carpathians (Ukraine), where stromatactis occurs within a microcrystalline host and grades into red nodular limestones of Rosso Ammonitico type (Fig. 17).

Stromatactis: a specific early diagenetic phenomenon

The different occurrences of the stromatactis phenomenon, although with relative portions of diagnostic features varying from place to place, have in common a specific system of cavities formed in a marine carbonate deposit, which under marine-phreatic conditions became infiltrated by internal sediments, accompanied or followed by marine cement precipitation (Bathurst 1982; Bourque and Boulvain 1993). Here, we support

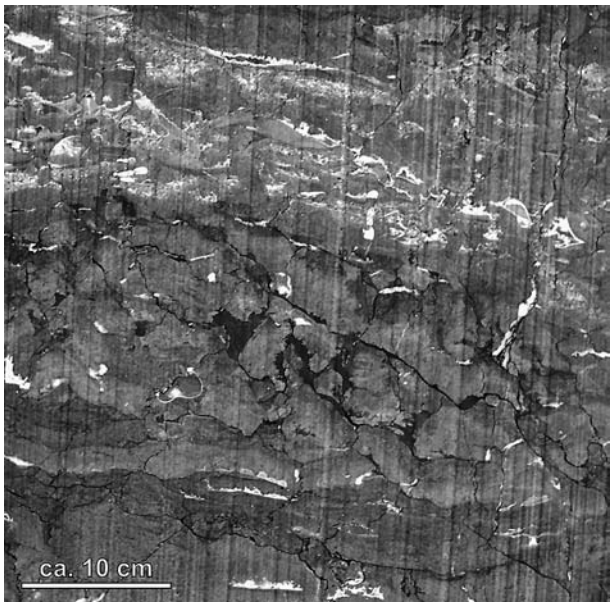

Fig. 17 Red stromatactis limestones in lateral and vertical contact with red nodular limestones (Rosso Ammonitico type), Middle Jurassic, southern Ukraine Pieniny klippen belt. Such relationships demonstrate that stromatactis facies is an essential option during Jurassic drowning intervals. In general, stromatactis facies are bounded by a drowning unconformity, crinoidal sands and/or (hemi-)pelagic facies. Important aspects of formation and preservation, such as **a** the establishment of siliceous sponge communities, **b** syneresis with its possible relation to the early stages of chert formation, **c** the importance of redox-cycling (organic matter, iron), and **d** related time constraints or subsidence rates, remain to be explored

Bathurst's view in defense of a particular early diagenetic pathway that remains to be explored, instead of being blurred by an inconsistent extension of the term's definition or an interpretation too general.

Although some features of stromatactis superficially resemble those found in modern methane hydrate deposits, so far not one occurrence exists where petrographic evidence for stromatactis is associated with geochemical evidence of either methanogenesis or methane oxidation. In contrast, in stromatactis normal-marine isotopic composition is the rule throughout, and where ^{13}C-depleted carbonates are present (e.g., Peckmann et al. 2002; Peckmann and Thiel 2004), the related rock fabrics simply do not match the definition. Krause (2001) has proposed a relationship of (true) stromatactis with CO_2 gas hydrates. However, his statement is inconsistent with any reasonable pCO_2, TCO_2, or related depth–pressure calculations as so convincingly demonstrated, for example, by DiFilippo et al. (2003). Indeed, and as confirmed with the application of advanced geochemical methods such as carbon and oxygen isotope (e.g. Boulvain 1993, 2001; Bourque and Raymond 1994) and strontium isotope chemistry (e.g., Kaufmann and Wendt 2000), or rare earth element patterns (this paper), Bathurst's (1982) view that stromatactis remains to be explained in terms of early diagenesis under normal-marine conditions stands untouched.

Significance of Arzo stromatactis limestones

Petrographically and geochemically, our results introduce the Arzo locality as an unequivocal example of a Mesozoic red stromatactis limestone. Palaeobiologically, it matches the common stromatactis sponge consortium. In addition, it displays good evidence for the crucial role of the decay of organic tissue inducing contraction of an organic medium and sediment shrinkage patterns, sagging and collapse features, siliceous sponge calcification, and patchy sediment lithification. The relationship between stromatactis and neptunian dykes is locally coincidental but apparently unrelated in terms of cause to effect.

Arzo stromatactis limestones, as the entire Broccatello unit, lack unequivocal evidence for photoautotrophic organisms. Instead, the community of siliceous sponges associated with brachiopods, crinoids, calcareous sponges, terebellids, and molluscs must be considered to represent the deep-water endmember of an effective Liassic benthic carbonate factory (see Krautter 1996 and Neuweiler et al. 2001b for other types of Liassic sponge accumulations). Geochemically, marine-oxic conditions are prevalent. Oxygen and carbon stable isotopic compositions do not deviate significantly from the inferred normal-marine values, and no indications for hydrothermal circulation or seepage of hydrocarbons have been found. The REE + Y patterns clearly document an early benthic-diagenetic, shallow subsurface environment for the evolution of the stromatactid cavity system.

Instead of thinking in terms of replacive diagenesis, seepage fluid flow, or clathrate formation and dissociation, we are confident that stromatactis mirrors a type of syneresis feature. This view of a maturation process of a particulate gel (in the sense of a colloidal polymeric suspension, e.g., Brinker and Scherer 1990; Larson 1999; see also Dewhurst et al. 1999) is consistent with successive decay and shrinkage features (phase separation), molecular evidence for former marine microgels or colloids in mud-mound automicrites (Neuweiler et al. 2000, 2003), and abnormal yield stresses requiring a cohesive medium to stabilize mound slopes of carbonate mud supporting depositional dips of up to 25° (e.g. Bathurst 1982; Boulvain 1993). In addition, considering syneresis might help to explain occasional fluid escape structures (Monty 1995) from exuding solvents, and the strong preference of stromatactis to occur in fine-grained sediment hosts. Indeed, cavity opening during syneresis would be likely inhibited within poorly sorted carbonate sands in view of the higher degree of internal friction (yield stress).

Conclusions

1. The Lower Liassic (essentially Lower Sinemurian) Broccatello unit of Arzo (southern Alps, southern Switzerland) contains patches of red stromatactis limestones. Like their Palaeozoic analogues, the

stromatactis limestones are relatively fine-grained and match the common stromatactis siliceous sponge consortium.

2. Palaeobiologically, petrographically and geochemically, the identified sedimentary and diagenetic environments encompass: (a) a subphotic benthic community of active and passive filter feeders within an essentially oxic, marine environment, (b) a complex shallow subsurface, early-diagenetic environment with organic matter transformation, sediment shrinkage, aragonite dissolution, SiO_2 dissolution, calcification, REE remobilization, in-situ collapse, and first generations of sediment infiltration, (c) a rather simple, shallow-burial marine-phreatic environment of marine cement precipitation in association with sediment infiltration, with crinoid meadows under current active, open water conditions above, (d) a shallow to middepth burial environment of the main multigeneration dyke and breccia formation with their related successions of internal sediment and cement fill, (e) a middepth burial environment with sediment injection of (Pliensbachian) marly lime mud, and (f) a late diagenetic burial environment with calcite cementation, pressure dissolution, and calcite veining at maximum temperatures of about 60°C.
3. The stromatactis cavity system evolved early during the complex shallow subsurface diagenetic pathway and was connected to the system of moldic porosity. It remained open, or reopened via syn-sedimentary tectonics until the late stages of burial diagenesis.
4. Because of the complexity of the fabrics involved, stromatactis is considered to represent a specific natural phenomenon, meanwhile with a significant number of well-documented Mesozoic examples. Stromatactis limestones appear as an essential option during the early stages of postdrowning intervals, whereas the detailed parameters favoring realization or inhibition remain to be explored.
5. The chronological succession and the characteristics of the different fabrics, combined with their inorganic and organic chemical signatures, demonstrate the importance of syn-sedimentary deformation (syneresis) and mineral authigenesis acting simultaneously. Such a combination of processes might be related to highly reactive fluids inducing calcification from exuding solvent and a remaining, rather inert gel-like material.
6. Syneresis, i.e., the maturation of particulate polymer gels, not only explains shrinkage features, abnormal yield stresses, and occasional water escape structures, but also opens the perspective for experimental simulation, e.g., using silica polymer suspensions (cf. Cabane et al. 1997), studying phase separation (exuding solvent), and subsequent fate via contraction and oxidation in the shallow subsurface environment.

Acknowledgements F. Neuweiler acknowledges financial support from the Alexander-von-Humboldt Foundation via FNRS, Brussels, from the Deutsche Forschungsgemeinschaft project-no. NE652/3, the Neuweiler family (Rutesheim, Leonberg) for their broad-minded sponsoring of FN's research, and Michal Krobicki (University Krakov) for organizing a special field trip in the Ukraine. We are grateful to Frédéric Boulvain (Université Liège) for Fig. 1a; Klaus Simon (University Göttingen) for performing ICP-MS analyses, and Stefano Bernasconi (ETH Zürich) for carbon and oxygen isotope analysis. Journal reviewers' remarks by Pierre-André Bourque (University Laval, Québec, Canada) and Karen H. Johannesson (University of Texas at Arlington) helped to improve the original manuscript. Last but not least, Rudolf Reber and Gatto Gianola are thanked for their hospitality in Tremona.

References

Aubrecht R, Szulc J, Michalik J, Schlögl J, Wagreich M (2002) Middle Jurassic stromatactis mud-mound in the Pieniny Klippen Belt (Western Carpathians). Facies 47:113–126

Bathurst RGC (1982) Genesis of stromatactis cavities between submarine crusts in Palaeozoic carbonate mud buildups. J Geol Soc 139:165–181

Bau M (1996) Controls on the fractionation of isovalent trace elements in magmatic and aqueous systems: evidence from Y/Ho, Zr/Hf, and lanthanide tetrad effect. Contrib Mineral Petrol 123:323–333

Bau M, Dulski P (1999) Comparing Yttrium and rare earths in hydrothermal fluids from the Mid-Atlantic ridge: implications for Y and REE behaviour during near-vent mixing and for the Y/Ho ratio of Proterozoic seawater. Chem Geol 155:77–90

Bau M, Möller P, Dulski P (1996) Yttrium and lanthanides in eastern Mediterranean seawater and their fractionation during redox-cycling. Mar Chem 56:123–131

Baumgartner PO, Bernoulli D, Martire L (2001) Mesozoic pelagic facies of the Southern Alps: Paleotectonics and paleoceanography. In: IAS meeting 2001 Davos Excursion A1:1–19

Beauchamp B, Savard M (1992) Cretaceous chemosynthetic carbonate mounds in the Canadian Arctic. Palaios 7:434–450

Bernasconi S, Riva A (1993) Organic geochemistry and depositional environment of a hydrocarbon source rock: The Middle Triassic Grenzbitumenzone Formation, Southern Alps, Italy/Switzerland. In: Spencer AM (ed) Generation, accumulation and production of Europe's hydrocarbons III, Special Publication of the European Association of Petroleum Geoscientists, vol 3. Oxford University Press, pp 179–190

Bernoulli D (1964) Zur Geologie des Monte Generoso (Lombardische Alpen). Ein Beitrag zur Kenntnis der südalpinen Sedimente. Beitr Geol Karte Schweiz NF 118:134

Bernoulli D, Bertotti G, Froitzheim N (1990) Mesozoic faults and associated sediments in the Austroalpine-South Alpine passive continental margin. Mem Soc Geol It 45:25–38

Bertotti G, Picotti V, Bernoulli D, Castellarin A (1993) From rifting to drifting: tectonic evolution of the South-Alpine upper crust from the Triassic to the early Cretaceous. Sediment Geol 86:53–76

Bleck R (2002) An oceanic general circulation model framed in hybrid isopycnic-Cartesian coordinates. Ocean Model 4:55–88

Böhm F (1992) Mikrofazies und Ablagerungsmilieu des Lias und Dogger der Nordöstlichen Kalkalpen. Erlanger Geol Abh 121:57–217

Böhm F, Ebli O, Krystyn L, Lobitzer H, Rakus M, Siblik M (1999) Fauna, stratigraphy and depositional environment of the Hettangian-Sinemurian (early Jurassic) of Adnet (Salzburg, Austria). Abh Geol B -A. 56:143–271

Boulvain F (1993) Sédimentologie et diagenèse des monticules micritiques "F2j" du Frasnien de l'Ardenne. Serv Géol Belgique Prof Papers 260:427

Boulvain F (2001) Facies architecture and diagenesis of Belgian Late Frasnian carbonate mounds. Sediment Geol 145:269–294

Bourque P-A, Boulvain F (1993) A model for the origin and petrogenesis of the red stromatactis limestone of Paleozoic carbonate mounds. J Sed Petrol 63:607–619

Bourque P-A, Gignac H (1983) Sponge-constructed stromatactis mud mounds, Silurian of Gaspé, Québec. J Sed Petrol 53:521–532
Bourque P-A, Raymond L (1994) Diagenetic alteration of early marine cements of Upper Silurian stromatactis. Sedimentology 41:255–269
Bourrouilh R, Bourque P.-A, Dansereau P, Bourrouilh-Le Jan F, Weyant M (1998) Synsedimentary tectonics, mud mounds and sea-level changes on a Palaeozoic carbonate platform margin: a Devonian Montagne Noire example (France). Sediment Geol 118:95–118
Brinker CJ, Scherer GW (1990) Sol–gel science. The physics and chemistry of sol–gel processing. Academic Press, New York, p 912
Brunton FR, Dixon OA (1994) Siliceous sponge-microbe biotoc associations and their recurrence through the Phanerozoic as reef mound constructors. Palaios 9:370–387
Cabane B, Wong K, Lindner P, Lafuma F (1997) Shear induced gelation of colloidal dispersions. J Rheol 41:531–547
Castellarin A (1972) Evoluzione paleotettonica sinsedimentaria del limite tra ''Piattaforma Veneta'' e ''Bacino Lombardo'', a nord di Riva del Garda. Giorn Geol 38(2):11–212
Cruse AM, Lyons TW, Kidder DL (2000) Rare earth element behavior in phosphates and organic-rich host shales: an example from the Upper Carboniferous of mid-continent North America. In: Glenn CR, Prévôt-Lucas L, Lucas J (eds) Marine authigenesis: from global to microbial. SEPM Special Publication 66. SEPM, Tulsa, USA, pp 445–453
De Baar HJW, German CR, Elderfield H, Van Gaans P (1988) Rare earth element distributions in anoxic waters of the Cariaco Trench. Geochim Cosmochim Acta 52:1203–1219
Dewhurst DN, Cartwright JA, Lonergan, L (1999) The development of polygonal fault systems by syneresis of colloidal sediments. Mar Petrol Geol 16:793–810
DiFilippo EL, Hammond DE, Corsetti FA (2003) Geochemical constraints for coexisting CO_2 gas hydrate and calcite: implications for sheet cracks, stromatactis, zebra and tepee-like structures. Sediment Geol 160:1–6
Dromart G, Allemand P, Quiquerez A (1998) Calculating rates of syndepositional normal faulting in the western margin of the Mesozoic Subalpine Basin (south-east France). Basin Res 10:235–260
Dunoyer de Segonzac G, Bernoulli D (1976) Diagenèse et métamorphisme des argiles dans le Rhétien Sud-alpin et Austroalpin (Lombardie et Grisons). Bull Soc Géol France 18(7):1283–1293
Dupont E (1881) Sur l'origine des calcaires dévoniens de la Belgique. Bull Acad R Sci Belg 2:264–280
Elderfield H, Greaves MJ (1982) The rare earth elements in seawater. Nature 296:214–219
Flajs G, Hüssner H (1993) A microbial model for the Lower Devonian stromatactis mud mounds of the Montagne Noire (France). Facies 29:179–194
Flügel E, Steiger T (1981) An Upper Jurassic sponge-algal buildup from the northern Frankenalb, West Germany. In: Toomey DF (ed) European fossil reef models. SEPM Special Publication 30. SEPM, Tulsa, USA, pp 371–397
Frauenfelder A (1916) Beiträge zur Geologie der Tessiner Kalkalpen. Eclogae Geol Helv 14:247–367
Fritz GK (1958) Schwammstotzen, Tuberolithe und Schuttbreccien im Weißen Jura der Schwäbischen Alb. Arb. Geol. Inst. TH Stuttgart, N. F. 13, Stuttgart
Froget C (1976) Observations sur l'altération de la silice et des silicates au cours de la lithification carbonatée (Région Siculo-Tunisienne). Géol Méditerran 3:219–226
Golonka J (2000) Cambrian-Neogen plate tectonic maps. Uniwersytetu Jagiellonskiego, Kraków, p 125
Haley BA, Klinkhammer GP, McManus J (2004): Rare earth elements in pore waters of marine sediments. Geochim Cosmochim Acta 68:1265–1279
Heckel PH (1972): Possible inorganic origin for stromatactis in calcilutite mound in the Tully Limestone; Devonian of New York. J Sed Petrol 42:7–18
Hendry JP (1993) Calcite cementation during bacterial manganese, iron and sulphate reduction in Jurassic shallow marine carbonates. Sedimentology 40:87–106
Hongo Y, Nozaki Y (2001) Rare earth element geochemistry of hydrothermal deposits and *Calyptogena* shell from Iheya Ridge vent field, Okinawa Trough. Geochem J 35:347–354
Hovland M, Talbot M, Qvale H, Olaussen S, Aasberg L (1987) Methane-related carbonate cements in pockmarks of the North Sea. J Sed Petrol 57:881–892
Hsü K (1983) Neptunian dykes and their relation to the hydrothermal circulation of submarine hydrothermal systems. Geology 11:454–457
James NP, Bourque P-A (1992) Reefs and mounds. In: Walker RG, James NP (eds) Facies models, response to sea level change. Geological Association of Canada, St. John's, Canada, pp 323–347
James NP, Gravestock DI (1990) Lower Cambrian shelf and shelf margin buildups, Flinders Ranges, South Australia. Sedimentology 37:455–480
Kälin O, Trümpy D (1977) Sedimentation und Paläotektonik in den Südalpen: Zur triasisch-jurassischen Geschichte des Monte Nudo-Beckens. Eclogae Geol Helv 70:295–350
Kaufmann B, Wendt J (2000) Calcite cement successions in Middle Devonian (Givetian) carbonate mud buildups of the southern Ahnet Basin (Algerian Sahara). Carbonates Evaporites 15:149–161
Kim S-T, O'Neil JR (1997) Equilibrium and non-equilibrium oxygen isotope effects in synthetic carbonates. Geochim Cosmochim Acta 61:3461–3475
Krause F (2001) Genesis and geometry of the Meiklejohn Peak lime mud-mound, Bare Mountain Quadrangle, Nevada, USA: Ordovician limestone with submarine frost heave structures—a possible response to gas clathrate hydrate evolution. Sediment Geol 145:189–213
Krautter M (1996) Kieselschwämme aus dem unterjurassischen Misonekalk der Trento-Plattform (Südalpen): taxonomie und phylogenetische Relevanz. Paläont Z 70:301–313
Larson RG (1999) The structure and rheology of complex fluids. Oxford University Press, New York, p 663
Lecompte M (1937) Contribution à la connaissance des récifs du Dévonien de l'Ardenne. Sur la presence de structures conservés dans des efflorescences cristallines du type ''Stromatactis''. Bull Mus R Hist Nat Belg 13:1–14
Lecompte M (1954) Quelques donnés relatives à la genèse et aux caractères écologiques des ''récifs'' du Frasnien de l'Ardenne. Vol jubilaire Victor van Straelen I:153–181
Lees A (1964) The structure and origin of the Waulsortian (Lower Carboniferous) 'reefs' of west-central Eire. Philos Trans R Soc Lond B 247:483–531
Lees A, Miller J (1995) Waulsortian banks. In: Monty CLV, Bosence DWJ, Bridges PH, Pratt BR (eds) Carbonate mudmounds, their origin and evolution. Spec Publ Int Assoc Sed, vol 23. Blackwell, pp 191–271
Leys S (1999) The choanosome of hexactinellid sponges. Invert Biol 118:221–235
MacLeod KG, Irving AJ (1996) Correlation of cerium anomalies with indicators of paleoenvironment. J Sed Res 66:948–955
Manatschal G, Bernoulli D (1999) Architecture and tectonic evolution of nonvolcanic margins. Tectonics 18:1099–1119
Mathur AC (1975) A deeper water mud mound facies in the Alps. J Sed Petrol 45:787–793
Mazullo SJ, Bischoff WD, Lobitzer H (1990) Diagenesis of radiaxial fibrous calcites in a subunconformity, shallow-burial setting. Upper Triassic and Liassic, Northern Calcareous Alps, Austria. Sedimentology 37:407–425
McLennan SM (1989) Rare earth elements in sedimentary rocks: Influence of provenance and sedimentary processes. In: Lipin BR, McKay GA (eds) Geochemistry and mineralogy of rare earth elements. Mineral Soc Am Rev Mineral vol 21, pp 169–200
Montanari L (1969) Aspetti geologici del Lias di Gozzano (Lago d'Orta). Mem Soc Ital Sci Nat Mus Civico Storia Nat Milano 17:25–92

Monty CLV (1995) The rise and nature of carbonate mud-mounds: an introductory actualistic approach. In: Monty CLV, Bosence DWJ, Bridges PH, Pratt BR (eds) Carbonate mud-mounds, their origin and evolution. Spec Publ Int Assoc Sed, vol 23. Blackwell, pp 11–48

Nesbitt BE (1996) Applications of oxygen and hydrogen isotopes to exploration for hydrothermal mineralization. Soc Econ Geol Newslett 27:1–13

Neuweiler F, Rutsch M, Geipel G, Reimer A, Heise K-H (2000) Soluble humic substances from in situ precipitated microcrystalline calcium carbonate, internal sediment, and spar cement in a Cretaceous carbonate mud-mound. Geology 28:851–854

Neuweiler F, Bourque P-A, Boulvain F (2001a) Why is stromatactis so rare in Mesozoic carbonate mud mounds? Terra Nova 13:338–346

Neuweiler F, Mehdi M, Wilmsen M (2001b) Facies of Liassic sponge mounds, central High Atlas, Morocco. Facies 44:243–264

Neuweiler F, d'Orazio V, Immenhauser A,. Geipel G, Heise K-H, Cocozza C, Miano TM (2003) Fulvic acid-like organic compounds control nucleation of marine calcite under suboxic conditions. Geology 31:681–684

Peckmann J, Thiel V (2004) Carbon cycling at ancient methane-seeps. Chem Geol 205:443–467

Peckmann J, Goedert JL, Thiel V, Michaelis W, Reitner J (2002) A comprehensive approach to the study of methane-seep deposits from the Lincoln Creek Formation, western Washington state, USA. Sedimentology 49:855–873

Polovina JJ, Mitchum GT, Evans GT (1995) Decadal and basin-scale variation in mixed layer depth and the impact on biological production in the Central and North Pacific, 1960–88. Deep-Sea Res I 42:1701–1716

Reitner J, Schumann-Kindel G (1997) Pyrite in mineralised sponge tissue—product of sulfate reducing sponge related bacteria. In: Neuweiler F, Reitner J, Monty C (eds) Biosedimentology of microbial buildups IGCP Project No.380. In: Proceedings of 2nd Meeting Göttingen/Germany 1996. Facies 36:272–276

Reitner J, Neuweiler F, Gautret P (1995) Modern and fossil automicrites: Implications for mud mound genesis. Facies 32:2–17

Ross RJ, Jaanusson V, Friedman I (1975) Lithology and origin of Middle Ordovician calcareous mudmound at Meiklejohn Peak, southern Nevada. US Geol Survey Prof Pap 871:44

Schlager W (2003) Benthic carbonate factories of the Phanerozoic. In: Reijmer JJG, Betzler Chr, Mutti M (eds) New perspectives in carbonate sedimentology. Int J Earth Sci 92:445–464

Schumann-Kindel G, Bergbauer M, Manz W, Szewzyk U, Reitner J (1997) Aerobic and anaerobic microorganisms in modern sponges: a possible relationship to fossilization-processes. In: Neuweiler F, Reitner J, Monty C (eds) Biosedimentology of microbial buildups IGCP Project No.380. In: Proceedings of the 2nd Meeting Göttingen/Germany 1996. Facies 36:268–272

Shinn, EA (1968) Burrowing in recent lime sediments of Florida and the Bahamas. J Paleont 42:879–894

Stanton RJ Jr, Jeffery DL, Guillemette RN (2000) Oxygen minimum zone and internal waves as potential controls on location and growth of Waulsortian Mounds (Mississippian, Sacramento Mountains, New Mexico). Facies 42:161–176

Thiel V, Blumenberg M, Hefter J, Pape T, Pomponi S, Reed J, Reitner J, Wörheide G, Michaelis W (2002) A chemical view of the most ancient metazoa—biomarker chemotaxonomy of hexactinellid sponges. Naturwissenschaften 89:60–66

Tsien HH (1985) Origin of stromatactis—a replacement of colonial microbial accretion. In: Toomey DF, Nitecki MH (eds) Paleoalgology. Springer, Berlin Heidelberg New York, pp 274–289

Veizer J, Ala D, Azmy K, Bruckschen P, Buhl D, Bruhn F, Carden GAF, Diener A, Ebneth S, Goddéris Y, Jasper T, Korte C, Pawellek F, Podlaha OG, Strauss H (1999) $^{87}Sr/^{86}Sr$, $\delta^{13}C$ and $\delta^{18}O$ evolution of Phanerozoic seawater. Chem Geol 161:59–88

Wallace MW (1987) The role of internal erosion and sedimentation in the formation of stromatactis mudstones and associated lithologies. J Sed Petrol 57:695–700

Wendt J, Kaufmann B, Belka Z (2001) An exhumed Palaeozoic underwater scenery: the Visean mud mounds of the eastern Anti-Atlas (Morocco). Sediment Geol 145:215–233

Wiedenmayer F (1963) Obere Trias bis mittlerer Lias zwischen Saltrio und Tremona (Lombardische Alpen)—die Wechselbeziehungen zwischen Stratigraphie, Sedimentologie und syngenetischer Tektonik. Eclogae Geol Helv 56:529–640

Wiedenmayer F (1977) Die Ammoniten des Besazio-Kalks. Schweiz Paläont Abh 98:169

Wiedenmayer F (1980) Spiculites and sponges in the Lower Jurassic of the Western Tethys. In: Hartmann WD, Wendt JW, Wiedenmayer F (eds) Living and fossil sponges. Sedimenta 8:135–145

Winterer EL, Metzler CV, Sarti M (1991) Neptunian dykes and associated breccias (Southern Alps, Italy and Switzerland): role of gravity gliding in open and closed systems. Sedimentology 38:381–404